Journal of Hydrology: Regional Studies 36 (2021) 100871

Contents lists available at ScienceDirect

Journal of Hydrology: Regional Studies

journal homepage: www.elsevier.com/locate/ejrh

Analysis of the groundwater flow system in a high-altitude headwater region under rapid climate warming: Lhasa River Basin, Tibetan Plateau

Jiachang Chen[a,b], Xingxing Kuang[b,c,*], Michele Lancia[b], Yingying Yao[d], Chunmiao Zheng[b]

[a] School of Environment, Harbin Institute of Technology, Harbin 150090, China
[b] Guangdong Provincial Key Laboratory of Soil and Groundwater Pollution Control, School of Environmental Science and Engineering, Southern University of Science and Technology, Shenzhen 518055, China
[c] Shenzhen Municipal Engineering Lab of Environmental IoT Technologies, School of Environmental Science and Engineering, Southern University of Science and Technology, Shenzhen 518055, China
[d] Department of Earth and Environmental Science, School of Human Settlements and Civil Engineering, Xi'an Jiaotong University, Xi'an, Shaanxi, China

A R T I C L E I N F O

Keywords:
Lhasa River Basin
Tibetan Plateau
Groundwater flow
Climate change
Numerical modeling

A B S T R A C T

Study region: Lhasa River Basin (LRB) on the Tibetan Plateau, China.
Study focus: Tibetan Plateau has been undergoing climate warming in the past five decades. The hydrological processes in the LRB, a representative alpine headwater region basin on the Tibetan Plateau, are changing in response to climate warming. However, characteristics of groundwater recharge and discharge and response of the groundwater flow system to future climate change in this region remain unclear. This study constructed a three-dimensional numerical model to simulate the groundwater flow variations under different future climate change scenarios.
New hydrological insights for the region: Approximately 13.6 % (~71.6 mm/yr) of annual precipitation recharges groundwater. Glacier meltwater recharge is 10 % of the total groundwater recharge across the entire LRB, and this proportion increases to 34.8 % in the Yangbajing sub-basin. More than 80 % of the groundwater circulates within 0~0.3 km below ground surface. The groundwater flow system is dominated by travel times between 10–100 years and flow path distances less than 10 km. The baseflow shows an increasing trend in response to future climate change, and the increasing trends range from 0.07 to 0.21 m^3/s per year under different future climate change scenarios. The baseflow variation indicates that wet year will become wetter and dry year will become drier in the future.

1. Introduction

Tibetan Plateau, known as the “Asian Water Tower”, is the source region of the five major rivers (i.e., Indus, Ganges, Brahmaputra, Yangtze, and Yellow Rivers) in Asia, feeding more than 1.4 billion people (~20 % of the world's population) in downstream areas

* Corresponding author at: Guangdong Provincial Key Laboratory of Soil and Groundwater Pollution Control, School of Environmental Science and Engineering, Southern University of Science and Technology, Shenzhen 518055, China.
E-mail address: kuangxx@sustech.edu.cn (X. Kuang).

https://doi.org/10.1016/j.ejrh.2021.100871
Received 7 January 2021; Received in revised form 27 June 2021; Accepted 6 July 2021
Available online 16 July 2021
2214-5818/

(Immerzeel et al., 2010). It is the most sensitive place in low-latitudes to and as the amplification of climate change (Duan and Wu, 2006; Liu and Chen, 2000; Zhang et al., 2013). Previous studies have shown that the Tibetan Plateau is experiencing a remarkable warming during the past 50 years (Kang et al., 2010; Kuang and Jiao, 2016; Bibi et al., 2018). The hydrosphere on the Tibetan Plateau has been affected significantly by the raising temperature, such as the rainfall changes (Gao et al., 2014), permafrost degradation (Cheng and Wu, 2007; Li et al., 2008; Chen et al., 2019), and glacier retreat (Xiao et al., 2007; Yao et al., 2012). These variations recharacterized the hydrological cycle; thus, redistributed the components of water recharge and discharge on the Tibetan Plateau (Yao et al., 2004; Bianduo et al., 2009). Therefore, investigating the hydrological cycle under climate change is meaningful for better water resources sustainability and ecosystem health on the plateau (Langridge and Daniels, 2017).

Groundwater is an important component of the hydrological cycle, serving as a water reservoir and providing considerable amount of water in both wet and dry seasons (Andermann et al., 2012). Water level drop has been found across the globe, which will potentially impact the aquatic ecosystem (de Graaf et al., 2019; Green et al., 2011; Jasechko and Perrone, 2021) while the groundwater storage shows an increasing trend on the Tibetan Plateau (Xiang et al., 2016). To investigate the response of groundwater to climate change, many numerical models have been constructed to simulate groundwater flow pattern and evaluate the potential effects of climate change on groundwater systems (Kirshen, 2002; Ge et al., 2011; Goderniaux et al., 2011; Cao et al., 2013; Yao et al., 2017). The warming climate accelerates the thawing of permafrost and retreating of glaciers, alters the hydraulic properties of the aquifers and the surface water-groundwater interactions (Kurylyk et al., 2014). On the Tibetan Plateau, glacier and permafrost are widely distributed and the interactions between groundwater and the cryosphere become more active than 30 years ago (Cheng and Jin, 2013; Cheng and Wu, 2007; Ma et al., 2017; Shi et al., 2020). In snowmelt-dominated regions, groundwater recharge and discharge are significantly affected by the rising temperature (Tague and Grant, 2009; Huss and Hock, 2018; Saberi et al., 2019; Shi et al., 2020). As permafrost area shrinks, meltwater is disrupting the topographically controlled groundwater flow pattern in the Tibetan Plateau and increasing

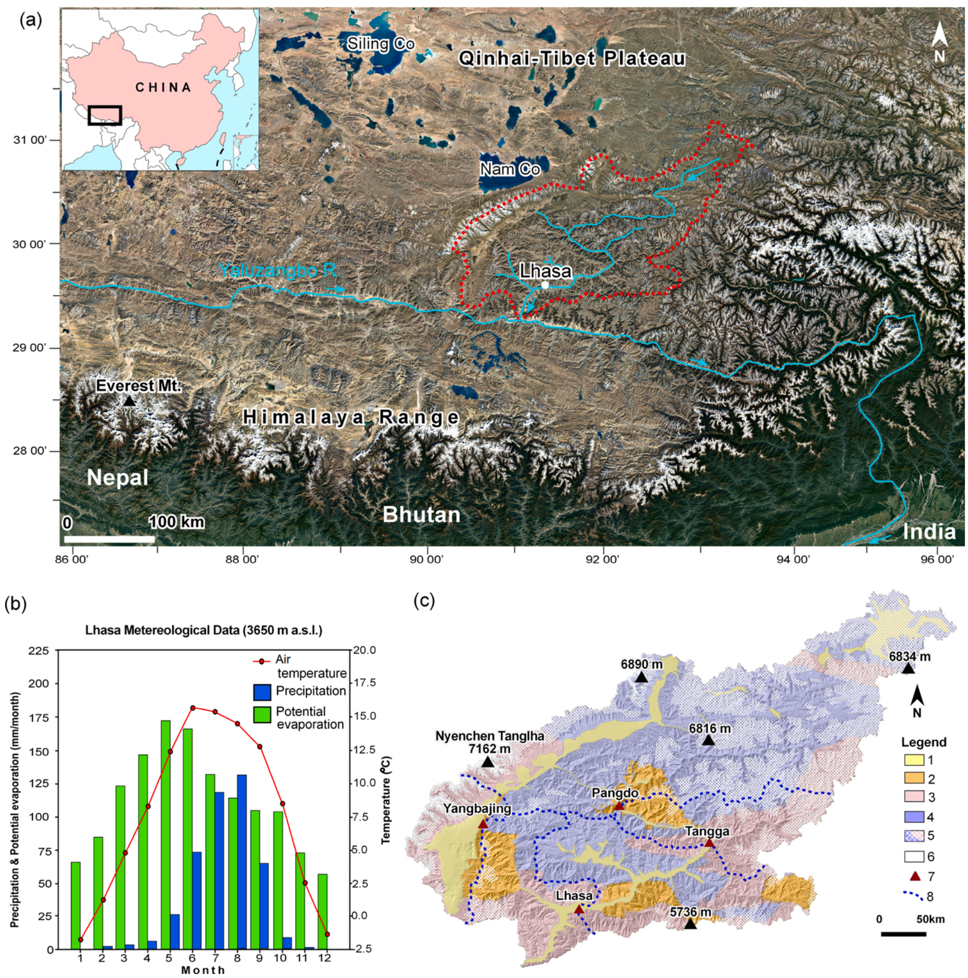

Fig. 1. Study area description: (a) satellite image (Google Earth) of the Tibetan Plateau, red dashed line indicates LRB; (b) Lhasa meteorological data from 1979 to 2000 (redrawn from Prasch, 2010); (c) aquifer map of LRB. Key to the legend: 1) alluvial aquifer; 2) volcanic and mélange zone aquifer; 3) granite aquifer; 4) terrigenous sequence aquifer; 5) permafrost; 6) glacier; 7) hydrological stations; 8) sub-basin dividing lines. (For interpretation of the references to colour in this figure legend, the reader is referred to the web version of this article).

the fraction of groundwater (baseflow) in runoff (Evans et al., 2015; Gao et al., 2021a; Gao et al., 2021b; Ran et al., 2021).

The LRB is a representative alpine catchment and a typical arid region on the Tibetan Plateau (Wu et al., 2005). Glacier meltwater has been shown to contribute 26 % of annual runoff, while groundwater contributes 28 % of the annual runoff (Liu, 1999). In the downstream reaches of the Yarlung Zangbo Basin, groundwater has been found to contribute approximately 27 % of the total river discharge (Yao et al., 2021). During the past two decades, there is a significant increase in runoff in the Lhasa River (Lin et al., 2008), reflecting the hydrological changes due to climate change. Liu et al. (2015) coupled the VIC (Variable Infiltration Capacity) model (Liang et al., 1996; Liang and Xie, 2001) with the optimization method of SCE-UA (Shuffled Complex Evolution developed at the University of Arizona) (Duan et al., 1994) to simulate the impacts of climate change on hydrological components such as evaporation, soil moisture, and runoff, and extrapolated these variations to the next 50 years in the LRB. Qiu et al. (2014) found that snowmelt water contributed 3~6% to the total runoff in the LRB when the Snowmelt Runoff Model was employed based on the MODIS (Moderate-resolution Imaging Spectroradiometer) data. The simulations show an increasing trend in runoff but the magnitudes of increase vary spatially and temporally. Hu and Jiao (2015) constructed a groundwater flow model in the Qaidam Basin, northern Tibetan Plateau via data derived from GRACE (Gravity Recovery and Climate Experiment), but this approach is not applicable in the LRB as the spatial resolution is too low. Groundwater studies in the LRB are limited, and the groundwater flow changes in response to climate warming remain unknown. In such an alpine area, numerical modeling is an effective tool to investigate the groundwater flow patterns, characterize groundwater recharge and discharge, and project the change of the groundwater flow system in response to future climate change.

In this study, a three-dimensional numerical groundwater flow model has been built for the LRB, combining precipitation, evapotranspiration, glacier, and permafrost. The presented model is further calibrated via observed baseflow and water table measurements. The purposes of this study are to (1) characterize the flow pattern and quantifying recharge and discharge of groundwater in the LRB, (2) investigate the contribution of baseflow to runoff, and (3) simulate the effects of future climate change on the groundwater flow system in the LRB. A sensitivity analysis has also been conducted to investigate the effect of model parameters on the modeling results. This is the first high resolution groundwater flow model coupled with glaciers and future climate change in the LRB.

2. Materials and methods

2.1. Site description

Lhasa River is one of the main tributaries of the Yarlung Zangbo River, located in the southern Tibetan Plateau. It is originated in the central part of the Nyenchen Tanglha Mountains, with a river length of about 551 km (Fig. 1a) (Wu et al., 2019). The LRB, covering an area of 32,526 km^2, is located within the latitudes of 29°20′~31°18′N and longitudes of 90°04′~93°21′E (Shi et al., 2014). Elevations of the region range from 3500 to 7000 m above mean sea level, with a mean altitude of over 4000 m and an average river channel gradient of 0.29 % (Chen et al., 2019). Lhasa is the capital city of the Tibet Autonomous Region, with population of 2.7 million and the highest degree of urbanization (Peng 2010). There are four hydrological stations in the LRB, governing four sub-basins respectively (Fig. 1c). Pangdo, Tangga, and Lhasa stations are located in sequence along the mainstream of the Lhasa River, and the Yangbajing station is situated in a tributary joining the Lhasa River downstream the Lhasa city (Peng and Du, 2010; Qiu et al., 2014).

The spatial and temporal distributions of climate factors in the LRB are nonuniform during the year. Annual mean air temperature of the LRB is 7.7 °C and annual mean precipitation is 437.8 mm (Fig. 1b), both gradually decreasing from South to North (Liu et al., 2019). The hottest and wettest months are June to August, because of the monsoon storms occurring from April to October (Prasch, 2010; Liu et al., 2019). According to the meteorological features, May to October can be regarded as the summer-hot season and November to April in the next year as winter-dry season (Bookhagen and Burbank, 2010). Most of the rainfall is distributed in the summer-hot season, accounting for approximately 95 % of the annual precipitation (Shi et al., 2014).

The total glacierized area in the LRB is 656 km^2, accounting for ~2% of the total area of the LRB (Table 1), including discontinuous glaciers in the upper Lhasa River and continuous glaciers in the northwestern mountain ranges (Liu, 1999; Prasch, 2010). Glaciers are mainly found in high elevation (>4000 m) areas, especially the northwestern watershed along the Nyenchen Tanglha Mountains. Permafrost is detected in the upper basin with altitude over than ~4800 m (Liu et al., 2011).

There are 6 land use types on the LRB, including farmland, grassland, forest, water body, urban, and unused land. About 60 % of the LRB is covered by grassland, with an area of 20,010 km^2 (Fig. 2). The second largest land use type is unused land, covering ~30 % of the total area, and the rest land use types take up 10 %.

Table 1
Hydrological stations in the LRB and observed annual runoff (Prasch, 2010).

Monitoring Point	Area (km^2)	Glacierized Area (%)	Annual Runoff (m^3/s)
Yangbajing	2654	11.5	23
Pangdo	16,416	2.0	204
Tangga	19,940	1.7	237
Lhasa	26,248	1.3	279

2.2. Data

The 90 m Shuttle Radar Topography Mission (SRTM) digital elevation model (DEM) was utilized to define surface topography and extract the catchment boundaries of the LRB. Geological map of the LRB is from Tibet Geological Survey (1979). The monthly data of precipitation and evaporation within the LRB during 1979~2000 were obtained from the China Meteorological Information Center (http://data.cma.cn/). Monthly runoff data at Pangdo, Tangga, Lhasa, and Yangbajing stations during 1979~2000 were collected from Institute of Tibetan Plateau Research. Runoff data during 2003–2014 were obtained from Huang et al. (2020). The water table data were obtained from pumping wells in the downtown Lhasa city, which are multi-year average data during 1979~2000. Distributions of glacier and permafrost were obtained from the Second Glacier Inventory Data Set of China (Zou et al., 2017). The land use and land cover data were obtained from National Tibetan Plateau Data Center (Liu, 2019). The future climate change scenarios were downloaded from the World Climate Research Programme CMIP6 (Coupled Model Intercomparison Project, Phase 6). The four climate change scenarios (SSP1−2.6, SSP2−4.5, SSP3−7.0, SSP5−8.5) used in model are the Tier-1, i.e., a higher simulated priority (O'Neill et al., 2016). The name of each scenario is a combination of the Shared Socioeconomic Pathways (SSPs) and the Representative Concentration Pathways (RCPs) (O'Neill et al., 2016). More details about the four climate change scenarios were provided in the supplementary material.

2.3. Baseflow separation

As LRB is vast and only limited water table monitoring data are available, baseflow is an important indicator to calibrate the groundwater flow model. Previous studies show that baseflow is the main constrain to calibrate a groundwater flow model (Okello et al., 2018; Zhang et al., 2014). Although there are many baseflow separation methods in the literature (e.g., Price, 2011; Yang et al., 2019), the methods are not verified in the LRB. Because of the complicated hydrological processes, the constructed model simply assumed the winter-dry season streamflow as baseflow, when precipitation is limited and snowmelt water is rare (Walvoord et al., 2012). Similar studies also used the winter season streamflow as baseflow (Singh and Jain, 2003; Tongal et al., 2013). According to the calculation results, the baseflow of Lhasa River accounts for 26.3 % of the runoff, which is similar to the result (~28 %) of isotope and chemistry baseflow separation method (Liu, 1999).

2.4. Hydrogeological parameters

Hydrogeology of the LRB was simplified from the geological map of the Tibet (scale 1:1,000,000). Geological profiles, stratigraphic profiles, and hydrogeological map of each model layer were obtained from the geological map and integrated into the groundwater flow model (Fig. 1c). Hydrogeology of the region can be simplified into four units: the alluvial sequence (Quaternary), volcanic and mélange clastic sequences (Upper Mesozoic to Paleogene), granite intrusion (Upper Mesozoic to Paleogene) and terrigenous sequence (Paleozoic to Mesozoic) (Figs. S1 and S2). Hydraulic conductivity of the units was initially estimated from empirical values that are

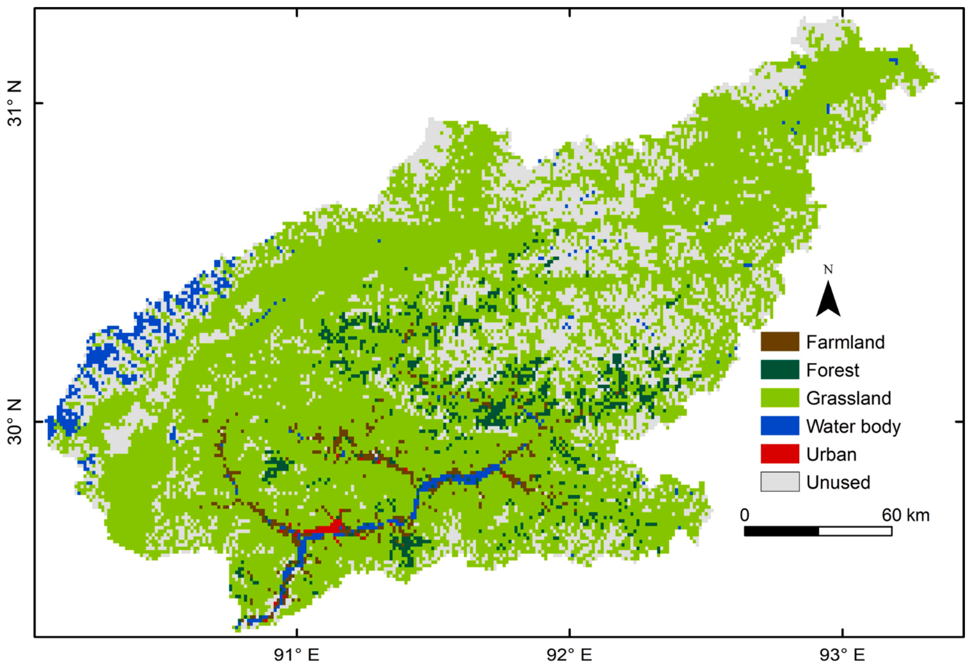

Fig. 2. Land use distribution on the LRB in 2000.

reported in previous studies (Ge et al., 2008; Gleeson et al., 2011) and slightly modified during model calibration (Table 2). Decrease of hydraulic conductivity with depth was included in the model and the depth dependent hydraulic conductivity is described by the integrated model (Kuang and Jiao, 2014):

$$\log k = \log k_r + (\log k_s - \log k_r)(1+z)^{-\beta} \tag{1}$$

where k_r is the residual permeability ($\log k_r$ is suggested to be -25.4 m^2 for Earth's continental crust in general), k_s is the surface permeability, β is the decay index, and z is the depth below ground surface. This model provides improved fit to the measured permeability data and can be used to describe the permeability-depth relationship through the entire Earth's crust (Kuang and Jiao, 2014). The permeability can be transformed to hydraulic conductivity K by (Fetter, 2001):

$$K = k\rho g/\mu \tag{2}$$

where ρ is the water density, g is the gravitational acceleration, and μ is the dynamic viscosity at 15 °C. Other parameters including specific storage (S_s) and specific yield (S_y) are also listed in Table 2.

2.5. Numerical model

The three-dimensional groundwater flow model was built based on the geological and land use maps of the LRB, using the finite-difference code MODFLOW-2005 (Harbaugh, 2005) with the NWT solution (Niswonger et al., 2011). The model was first built in steady-state and then converted to transient state after calibration. The steady-state model represents a long-term averaged condition and was used to figure out the groundwater flow pattern and water budget in the LRB. The transient model aims to forecast the evolution of the groundwater flow system under different future climate change scenarios.

The model is ~2.8 km thick in average and was discretized into 10 layers (Table S1). The thickness of the model layers ranges from 5 m of surface layer to 500 m of the deepest layer. Each layer's thickness increases exponentially with depth and layers under mountain areas are thickened while layers beneath valleys are thinned (Yao et al., 2017). Such model layer setup can improve the simulation accuracy of near-surface active layer and ensure groundwater flow within 2 km depth can be modeled adequately (Ge et al., 2008). There are 219 rows and 323 columns in each model layer, and the model was discretized to 707,370 cells with 1 km × 1 km resolution.

The lateral boundaries on the LRB's east, west, and north were specified as no-flow conditions (Fig. S3). The boundary type on the south is not clear because the basin topography is higher in the north and lower in the south, and cross-basin groundwater exchange may occur near the southern boundary as deep groundwater flow (Yao et al., 2017). The southern lateral boundaries were set as a specified flux boundary and the groundwater exchange through this boundary can be changed in the model calibration (Fig. S3). Groundwater recharge was specified on the top layer of the model, indicating the portion of rainfall or snowfall meltwater that infiltrates through the unsaturated zone and reach the water table. Infiltration coefficient of precipitation (α), i.e., ratio of groundwater recharge to precipitation, is one of the main parameters controlling groundwater recharge rate. In this model, the parameter α depends on the topsoil texture, which means land use of the LRB (Fig. 2) is the main consideration when assigning α to the hydrological zones. Values of α in the model vary from 0.03 to 0.4 (Table 2), in consistence with the α values reported in a semiarid and arid area similar to the LRB (Scanlon et al., 2006).

Groundwater seepage to river in the form of baseflow and evapotranspiration (ET) are the main ways of discharge of the groundwater flow system. Drainage network was extracted from the hydrological analysis based on DEM using QGIS (QGIS Development Team, 2020) and then discretized to the model grid. River stage and bed elevation were also obtained from the DEM. The evapotraspiration package (EVT) was used to simulate the transpiration effect of plants and direct evaporation that reduce the potential groundwater resources (Banta, 2000). Throughout the studied area, the maximum evaporation rate and the extinction depth are respectively 13.7 mm/yr and 4 mm/yr (Shi et al., 2014). At the southern boundary, the Yarlung Zangbo riverbed collects the regional groundwater flow and was characterized via specified flux boundary conditions. Groundwater flow was assessed in the first four layers characterized by sediments with high conductivities.

Glacier and permafrost distributions are important model inputs that can alter the groundwater recharge rate and hydraulic conductivity. Glaciations change the pressure overlying the aquifer and the ice melting rate during glacier receding or advancing, affecting the recharge and discharge relationships between groundwater and surface water (Provost et al., 2012). Given that the glaciers are increasingly retreating due to climate warming (Yao et al., 2012), glacier meltwater water is becoming a considerable resource in the LRB. Glacier's effect on groundwater can be regarded as a constant-head boundary condition (Boulton et al., 1995;

Table 2
Parameters in the validated model.

Land use type	α	Recharge rate (mm/yr)	Hydrogeological unit	Ks (m/d)	β	S_S (10^{-4} m^{-1})	Sy
Farmland	0.030	12.0~18.0	Alluvial	16.5	0.25	4.49	0.25
Forest	0.090	36.1~58.5	Granite	0.3	0.25	2.01	0.01
Grassland	0.115	45.4~83.5	Granite (weathered)	1.0	0.25	3.44	0.01
Water body	0.400	158.4~288.1	Terrigenous Sequence	0.3	0.25	2.26	0.01
Urban	0	0	Volcanics	5	0.25	3.65	0.01
Unused	0.210	82.8~152.4	Permafrost	0.001	/	1.13	0.01

Bense and Person, 2008; Cohen et al., 2010; Normani and Sykes, 2012; Mackay et al., 2020) or a constant-flux boundary condition (van Weert et al., 1997; Breemer et al., 2002; Carlson et al., 2007; Somers et al., 2019). In the model, a constant-flux boundary condition was assigned to the grids covered by glacier on the top layer and subsequently calibrated by the observed baseflow. This approach has been proven to be reasonable in numerical groundwater flow models with glaciation (van Weert et al., 1997; Breemer et al., 2002; Carlson et al., 2007; Lemieux et al., 2008; Markovich et al., 2016). Glacier recharge rate was assigned ~300 mm/yr (after calibration) as a constant-flux condition on the top layer where the glacier distributed, roughly equal to the annual precipitation. The glacier recharge rate was set as an initial estimation and then adjusted during the model calibration. Permafrost is generally a low permeability layer and treated as an aquitard by previous studies (Breemer et al., 2002; van Weert et al., 1997; Cheng and Jin, 2013; Wang et al., 2019). The cells located in permafrost area were assigned a hydraulic conductivity of 10^{-6} m/d initially (Ge et al., 2008), far lower than those of the aquifers. Cells within the seasonally frozen ground area were treated as normal grids (Kurylyk et al., 2016). The thickness of permafrost layer is 4~30 m, depending on the distance from the edge of the frozen ground (Feng, 2015).

2.6. Transient model

The steady-state model was changed into a transient model to predict the evolution of the groundwater system in response to future climate change. The model setting of the transient model is the same as that of the steady-state model. Changes of precipitation from the CMIP6 scenarios (SSP1−2.6, SSP2−4.5, SSP3−7.0, SSP5−8.5) were used as input for the transient model. Specific storage and specific yield were also added to the transient model (Table 2). Other parameters including hydraulic conductivity, infiltration rate, evapotranspiration, and glacier recharge remain the same as those in the steady-state model. The transient model simulates the evolution of the groundwater flow system in the next 80 years (2020–2100) under the four future climate change scenarios.

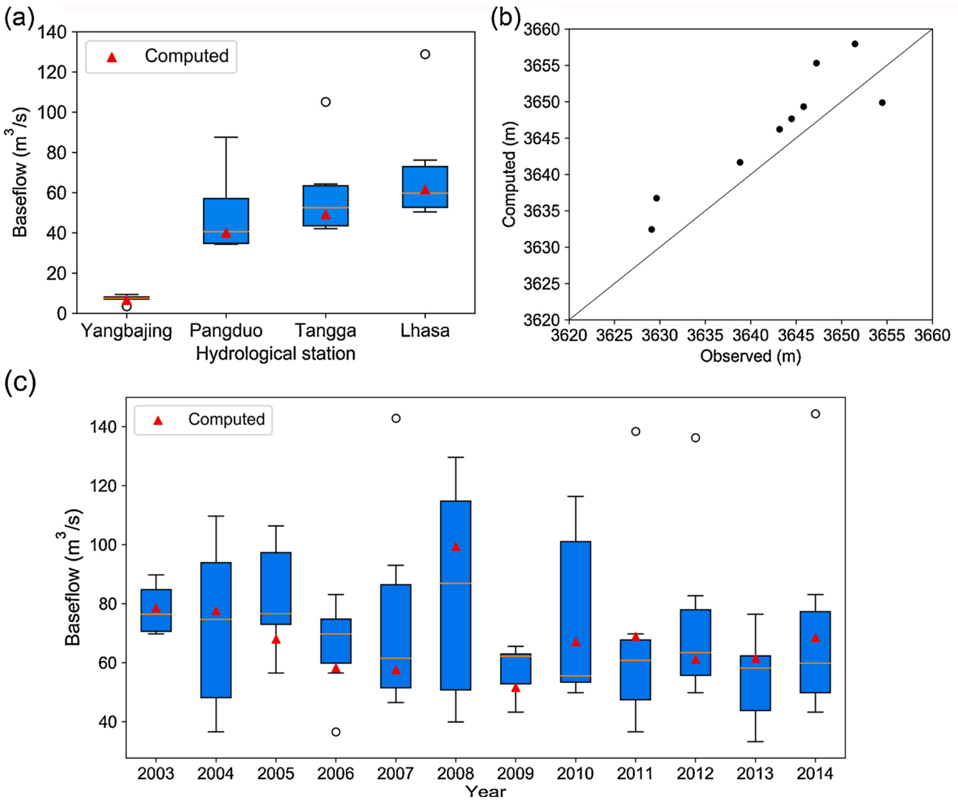

Fig. 3. Comparison of simulated and observed data. (a) Computed and observed baseflow at the four hydrological stations for the steady-state model. Red triangles are the computed baseflow from the steady-state model. Boxplot indicates observed streamflow in winter-dry period. Orange line within the box are the median; upper and lower box edges are upper quartiles and lower quartiles, respectively; sticks outside the box are upper limb and lower limb; open circles are abnormal values. (b) Computed and observed average (during 1979-2000) water tables in pumping wells in the Lhasa city for the steady-state model. (c) Computed and observed baseflow during 2003-2014 at the Lhasa hydrological station for the transient model. Red triangles are the computed baseflow from the transient model. Other symbols have the same meaning as Fig. 3a. (For interpretation of the references to colour in this figure legend, the reader is referred to the web version of this article).

3. Results

3.1. Model calibration

Parameters including hydraulic conductivity (*K*) and infiltration coefficient of precipitation (α) were first assigned and then adjusted during model calibration. Parameters that give the best agreement between simulated and observed data after calibration are listed in Table 2. Calibration followed the trial-and-error method, supported by the baseflow and water table observation data. Both the observed baseflow and water table measurements come from the winter-dry period, i.e., from November to April in the next year.

To evaluate the performance of the groundwater flow model, the absolute error (*AE*), relative error (*RE*), and the *Fit-NRMSE* (Yao et al., 2017) was used (Supplementary material). Fig. 3a shows the comparison between simulated and observed baseflow of the four sub-basins in the LRB for the steady-state model. The *RE* values vary from 1.7 % to 6.6 % and the *Fit-NRMSE* coefficient is 0.96. The simulated baseflow agrees well with the observed values. Fig. 3b presents a comparison of the simulated and observed water tables (multi-year average during 1979–2000) for the steady-state model. The *AE* values ranges from 2.84 to 8.08 with a mean of 3.67. The *Fit-NRMSE* coefficient is 0.80. All the observed water table data were obtained from pumping wells in the downtown Lhasa city, where the water table may be disturbed by pumping. The resolution of the grid (1 km $\times$ 1 km) is greater than the influence radius (~800 m) of

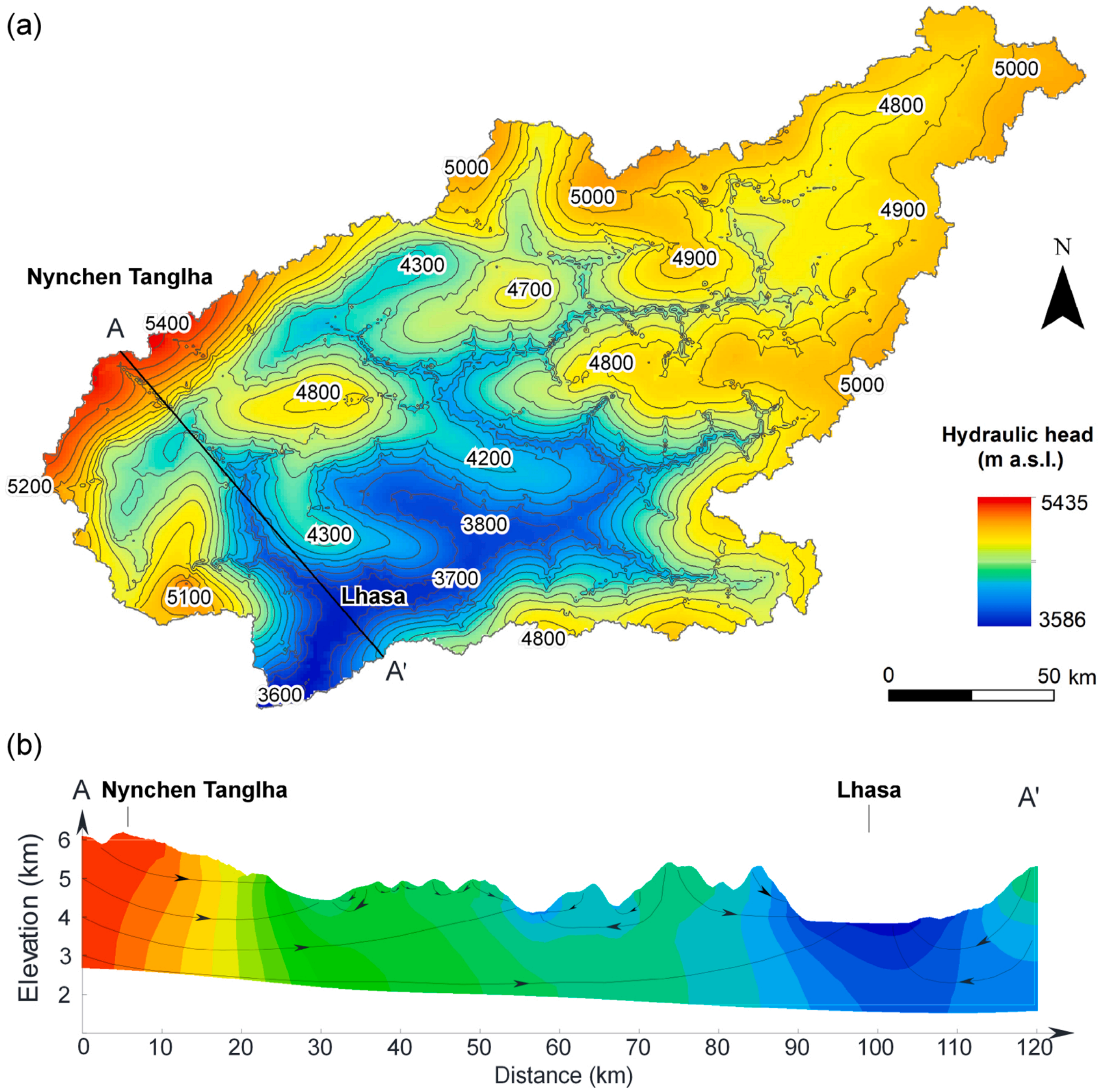

Fig. 4. Simulated hydraulic head distribution in the LRB: (a) hydraulic head contour map, labels indicate the elevation (m a.s.l.); (b) A-A' profile, arrows represent groundwater flow.

a extraction well (Wang and Wang, 2020). Thus, the computed water table should be higher than the observed water table values. As can be seen in Fig. 3b, most of the computed values are higher than the measured water tables, which shows that the model should be reliable. Fig. 3c presents a comparison of computed and observed baseflow during 2003–2014 at the Lhasa hydrological station for the transient model. The *RE* values vary from 2.7%–20.7% with an average of 10.8 % and the *Fit-NRMSE* coefficient is 0.74. Overall, the model calibration indicates that the model can provide reasonable and reliable results.

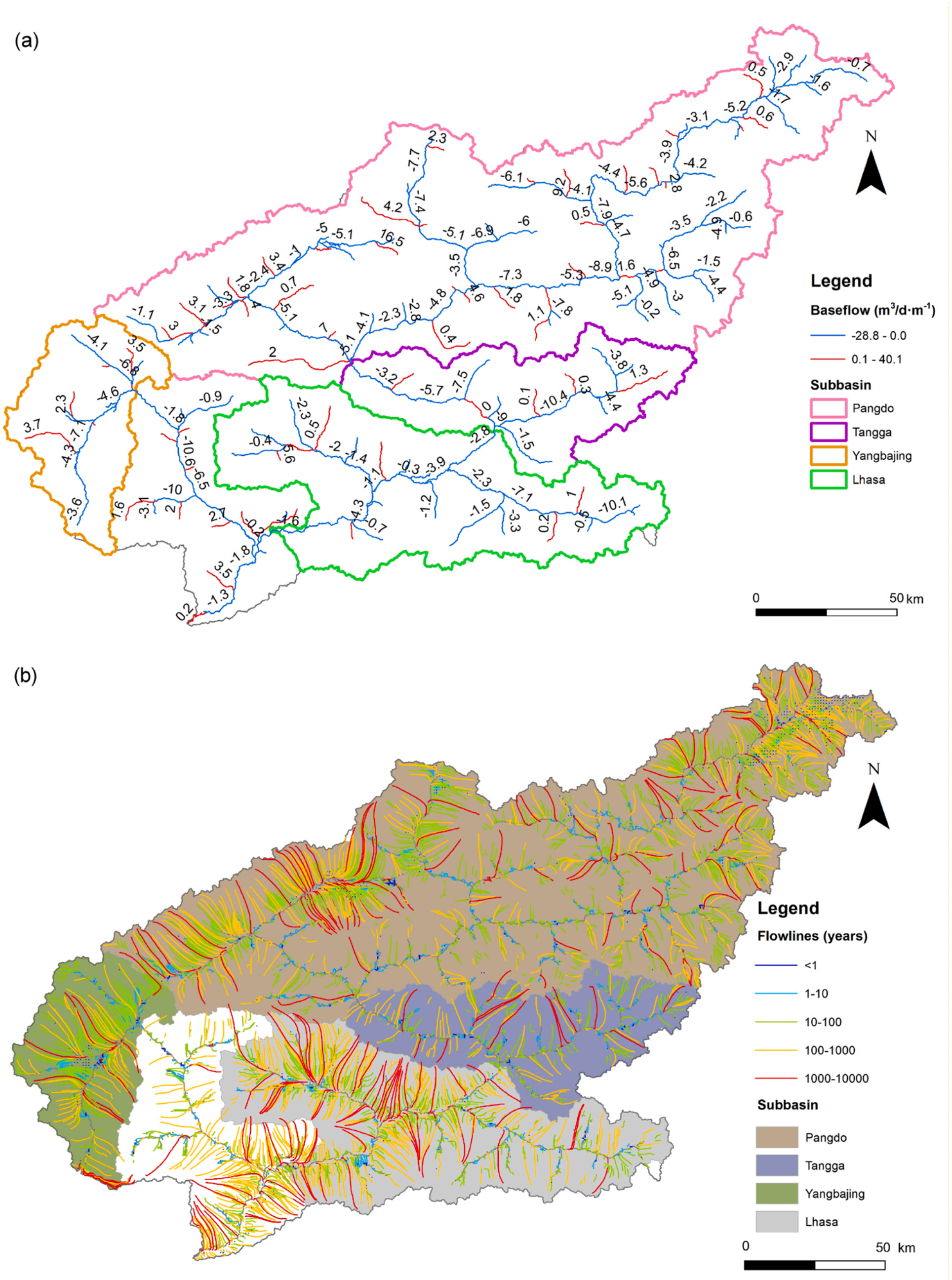

Fig. 5. Groundwater flow pattern on the Lhasa River Basin. (a) Interactions between groundwater and streamflow in each river section. Positive value (red line) means river feds groundwater, negative value (blue line) means groundwater discharges into river as baseflow. (b) Particle tracking of the groundwater in the 4 subbasins of Panddo, Tangga, Yangbajing, and Lhasa. (For interpretation of the references to colour in this figure legend, the reader is referred to the web version of this article).

3.2. Groundwater flow pattern

Hydraulic head distribution in the LRB is mainly controlled by topography and the hydrogeological setting as the hydraulic head variations are subdued version of the surface elevation (Fig. 4a). Simulated hydraulic heads decrease from northeast to southwest, in accordance with the topography. Such a hydraulic head distribution indicates a general northeast to southwest groundwater flow direction. The highest hydraulic head of 5435 m is located in the Nyenchen Tanglha Mountains in the western part of the basin, while the lowest hydraulic head of 3586 m is observed at the outlet of the LRB. These two points correspond to the highest and lowest elevations of the study area. The mean hydraulic gradient in the LRB is 2.9 %. Relatively high hydraulic gradients are located in the upper reaches of the basin. The greatest hydraulic gradient is up to 16 % in the mountain areas of eastern and western LRB near the divide. Hydraulic gradient in the central LRB becomes small as the slope decrease to 1% in this area, in correspondence of the Quaternary deposits characterized by relatively high hydraulic conductivities. A typical profile from the glacierized area through the Lhasa city showing the groundwater flow system is presented in Fig. 4b. The groundwater flow system is relatively complicated with both local and regional flowlines.

Variation of the infiltration coefficient of precipitation (α) depends on the different types of topsoils. Approximately 13.6 % of precipitation (~71.6 mm/yr) infiltrates into the saturated zone and become groundwater, among which 93.4 % discharges to streams as baseflow and 5.5 % returns to the atmosphere as evapotranspiration (~4.2 mm/yr). Only 1.1 % flows out through the southern boundary. More than 80 % of the groundwater flow is constrained within 0~0.3 km below ground surface.

Recharge of glacier meltwater to groundwater is not a significant component. The amount of groundwater recharge from glacier meltwater is 5.4 mm/yr, which is 7.1 % of the total groundwater recharge. For the Yangbajing sub-basin, in which glaciers are extensively distributed and the glaciers are retreating massively due to global warming (Yao et al., 2007, 2004), the simulated glacier melting rate is 29.1 mm/yr and accounting for 34.7 % of the total groundwater recharge.

Interactions between groundwater and surface water and the magnitude of exchange rates are shown in Fig. 5a. The positive value means water flow from river to groundwater, and the negative value means groundwater to river discharge. In most river reaches groundwater discharges into rivers as baseflow, with a magnitude of -28.8~0 m^3/d per meter. Relatively high discharge rates appear in the middle reaches of the Lhasa River. The river reaches with positive values indicate that the river water feed groundwater, where water level in the rivers should be higher than that of groundwater. The positive values are mostly distributed in the first-order tributaries in the upper stream of the Lhasa River, with magnitude of 0~40.1 m^3/d per meter.

A MODPATH analysis was carried out based on the MODFLOW simulation results (Fig. 5b). A total of 4536 pathlines were described where groundwater flow terminated by discharging to rivers, with particle tracking distances and tracking times. The shortest tracking distance is 0.5 km and the longest is 43.6 km. The particle tracking time ranges from 67 days to 753,482 years. The area with dense pathlines, such as the mid-southern LRB and depressions located at mountain front on the western LRB, gain more recharge from groundwater and the range of groundwater tracking time tends to be wider. Mountain areas in the Pando sub-basin, especially if permafrost is present, tend to have sparser and shorter pathlines, indicating short refreshing periods in these places and young groundwater ages. The particle tracking time is related to the tracking distance but there is not obvious functional relationship because of the various depth-dependent hydraulic conductivity (10^{-6}~10^{1} m/d). As shown in Fig. 6, tracking time between 10–100 years account for 52.6 % of the pathlines. The tracking distances less than 10 km long account for 85 % of the pathlines, which means local circulation plays a predominant role in groundwater flow.

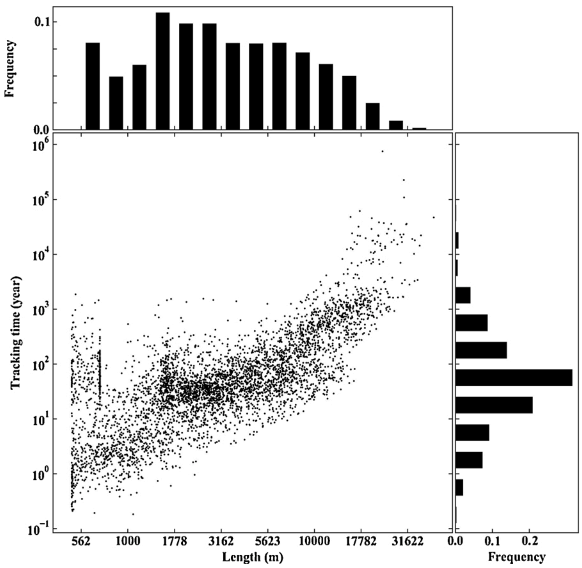

Fig. 6. The relationship between particle tracking distance and time. The vertical and horizontal histograms are the distribution of particles tracking times and distances, respectively.

3.3. Parameter sensitivity analysis

Infiltration recharge, hydraulic conductivity, aquifer thickness, and distance between surface water features are significant parameters for configuring water table (Haitjema and Mitchell-Bruker, 2005). A sensitivity analysis was carried out characterizing the hydraulic conductivity (K_s), ratio of horizontal to vertical hydraulic conductivity (K_h/K_v), infiltration coefficient of precipitation (α), decay index (β), glacier recharge, specific storage (S_s), specific yield (S_y), southern boundary discharge, hydraulic conductivity of permafrost, maximum evapotranspiration rate, and extinction depth (Table S2). The two model output variables of baseflow and hydraulic head were used to quantify how the model change with the input variables. Results of sensitivity analysis show that α and K_s affect the hydraulic head and baseflow the most (Table S2). The infiltration recharge and hydraulic conductivity are the main parameters during the model calibration. In this model, the infiltration recharge is mainly affected by the infiltration coefficient of precipitation (α) and the hydraulic conductivity is mainly affected by the decay index (β) in the permeability-depth model. Thus, the following sensitivity analysis is focused on the infiltration coefficient of precipitation (α) and the decay index (β).

The infiltration coefficient of precipitation (α) was set to vary between 0.03 to 0.40 for different land use types (Table 2). In the sensitivity analysis, α was changed 10 % for each land use type at each time. Fig. 7a shows the differences of baseflow in the four hydrological stations and average water table of the LRB varying α. As α increases, both baseflow and mean water table increase linearly. Meanwhile, the discharge percentage of baseflow and evapotranspiration are slightly increased and decreased with variation less than 5%, respectively. The discharge percentage of southern boundary discharge remains constantly at about 1%.

The decay index β controls the rate of decrease of permeability with depth (Kuang and Jiao, 2014). A sensitivity analysis on the decay index β was also conducted to evaluate its effect on groundwater flow. Kuang and Jiao (2014) suggested that for Earth's continental crust in general, the decay index β is equal to 0.25. The decay index β was set to vary from 0.1 to 0.45 in the sensitivity analysis (Fig. 7b). As β increases, permeability decreases faster with depth, thus leads to steepened groudwater table and reduces groundwater flow velocity according to the Darcy's law. The baseflow discharge decreases with β but the evapotranspiration and southern boundary discharge increases with β (Fig. 7b). Simulated hydraulic head distributions along the A-A' profile as β increases are shown in Fig. 8. As β increases, strata's permeability at great depths become smaller. Thus, the vertical velocity of groundwater flow decreases and less groundwater flows into deep aquifers. The decrease of strata's permeability will also lead to less groundwater discharge to the downstream areas, and the groundwater flow system also tends to be simpler.

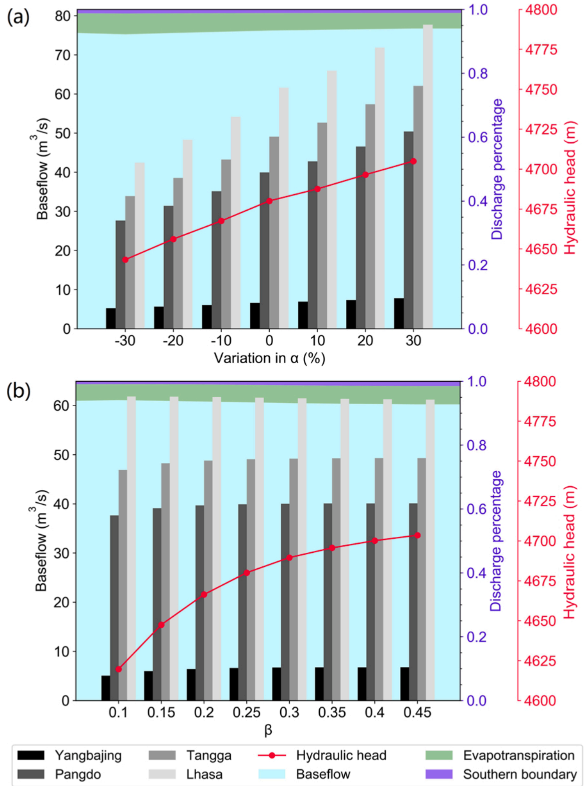

Fig. 7. Changes in baseflow in the four hydrological stations and mean water in the LRB with infiltration coefficient of precipitation (α) and the decay index (β). The discharge percentage is the ratio of baseflow, evapotranspiration or southern boundary discharge to the total groundwater discharge.

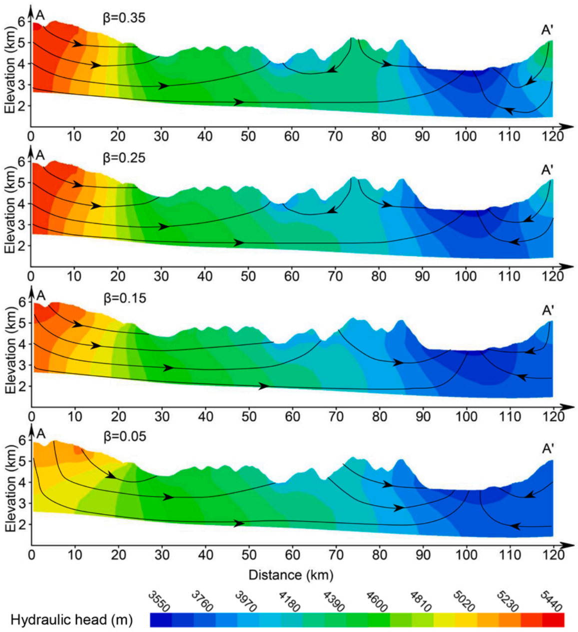

Fig. 8. Simulated hydraulic head distributions along the A-A' profile as β increases. The decay index β in the permeability-depth function controls the decreasing rate of permeability with depth. Greater β indicates faster decrease of permeability with depth.

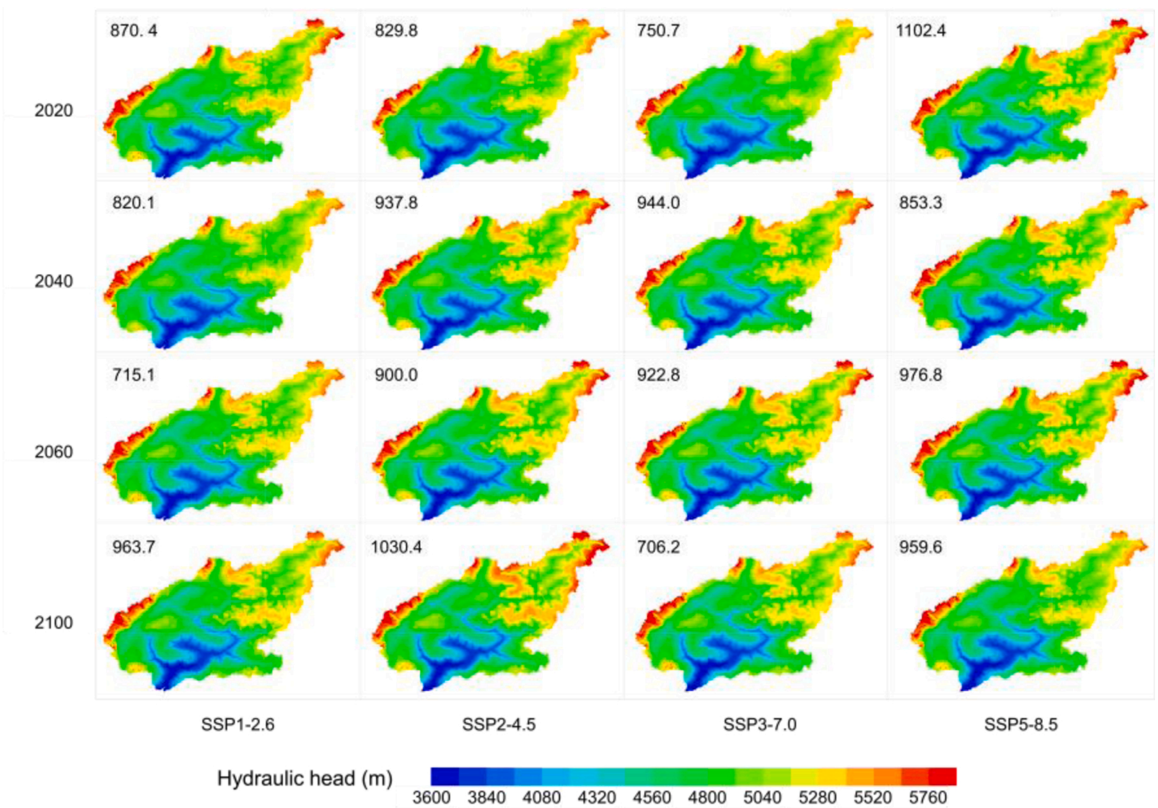

Fig. 9. Simulated distribution of hydraulic head in the LRB for typical four years (2020, 2040, 2060, 2100) by the transient model. The number on the upper-left corner of each subplot represents the annual precipitation for the corresponding scenario, with unit of mm.

3.4. Groundwater flow system in the next 80 years (2020~2100)

The groundwater flow system was simulated for the next 80 years (2020–2100) based on the future climate scenarios using the transient model. The four climate change scenarios show different trends in annual air temperature during 2020–2100 (Fig. S4). A combination of groundwater flow patterns in the four scenarios in four typical years (2020, 2040, 2060, 2100) is shown in Fig. 9. Hydraulic head in the whole basin is related to precipitation. Under the same future climate change scenario, higher precipitation corresponds to higher hydraulic head in the basin. The variations of the hydraulic heads in the high-altitude areas also becomes more significant. The rise of hydraulic head in mountainous areas (upstream sectors and the Nyenchen Tanglha Mountains) is greater than that of the other areas, indicating that changes in groundwater flow system in high mountain areas are greater than the other areas. The results also imply that the groundwater flow system in high mountain areas is more sensitive to climate change.

Fig. 10 shows the variations of baseflow and hydraulic head under the four future climate change scenarios. The period of 1998–2014 represents the past and 2020–2100 represents the future. The past and future annual precipitation data were obtained from observation and the CMIP6 climate change scenarios. The baseflow and hydraulic head fluctuate with the variation of future annual precipitation. The baseflow shows increase trends under the four climate change scenarios, and the increase trends range from 0.07 to 0.21 m^3/s per year (Table 3). The baseflow shows the greatest increasing trend in SSP5−8.5 and the smallest trend in SSP1−2.6. The mean hydraulic head also increases with the precipitation increment. The greatest increase in hydraulic head is also in SSP5−8.5 as the smallest occurs within SSP1−2.6. The magnitude of variation in baseflow becomes greater after about 2035, which indicates that wet year will become wetter and dry year will become drier in the future (Fig. 10). Extremely high precipitation and corresponding high hydraulic head and baseflow will become more frequently than the past, and the change of groundwater flow system will be intensified in the future.

4. Discussion

4.1. Model uncertainties

Uncertainties analysis of the model is based on the sensitivity analysis. Results of the sensitivity analysis show that α is the most sensitive factors affecting baseflow in the LRB (Table S2). Glacier recharge and surface hydraulic conductivity K_s are also sensitive factors affecting the baseflow (Table S2). Baseflow increase in the LRB is predictable in the future result from the climate warming. Surface hydraulic conductivity (K_s) affects the hydraulic head the most, and glacier recharge is the next.

In the transient model, glacier and permafrost are constant inputs. From the results of uncertainty analysis, the hydraulic conductivity of permafrost has the smallest effect on both baseflow and hydraulic head among all the input values, so ignoring the changes of permafrost has an almost null impact on the model. However, glacier recharge is the second significant factors affecting the groundwater flow model. The largest uncertainty of the transient model comes from glacier recharge. The glacier recharge rate in the transient model for prediction uses the historical value, i.e., the glacier recharge rate averaged from 1979~2000. Uncertainty of the transient model is mainly due to the difference in the glacier recharge rates between the past and the future. According to the trend of temperature change in the Lhasa River Basin, the annual warming rate from 1979 to 2000 is 0.053 ℃/year, while the annual warming rate from 2003 to 2014 is 0.067 ℃/year with the maximum and minimum value of 1.3 ℃/year and -0.78 ℃/year, respectively.

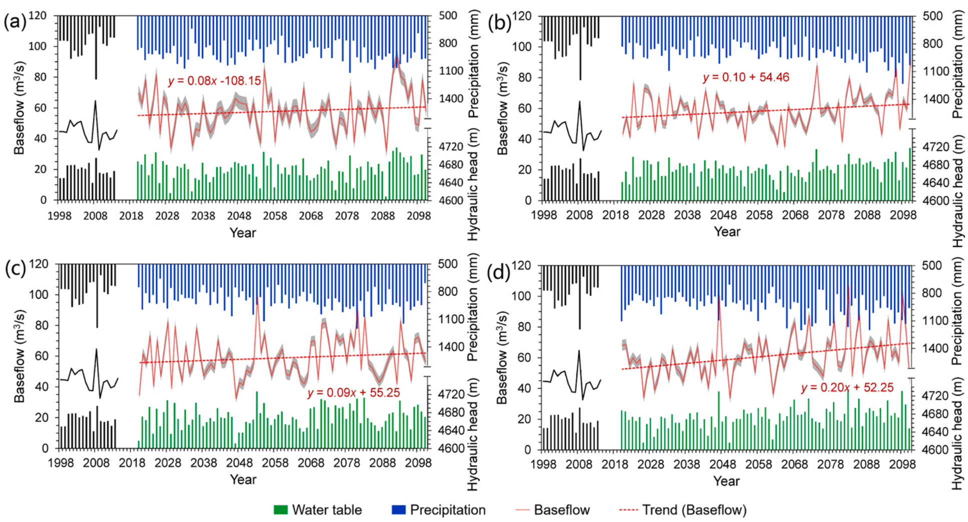

Fig. 10. Variations of baseflow and water table under different future climate change scenarios of SSP1−2.6 (a), SSP2−4.5 (b), SSP3−7.0 (c), and SSP5−8.5 (d) respectively. The black color represents the variation in the past (1998~2014) and the other colors represent the variation in the future (2020~2100).

Table 3
Trend in precipitation, baseflow, and mean hydraulic head in the past (1998~2014) and in the next 80 years (2020~2100).

Trend	1998~2014	2020~2100			
		SSP1−2.6	SSP2−4.5	SSP3−7.0	SSP5−8.5
Precipitation(mm/yr)	−3.96	0.52	1.58	1.33	1.84
Baseflow ($m^3 \cdot s^{-1} \cdot yr^{-1}$)	−0.35	0.07	0.11	0.08	0.21
Hydraulic head (m/yr)	−4.18	0.10	0.19	0.17	0.37

Assuming that the trend of glacier melt and recharge is consistent with the trend of temperature, the rate of glacier recharge varies by ±26.4 %, leading to the uncertainty of about 141007.7 m^3/d (~2.1 %) in baseflow and 2.1 m (<0.1 %) in hydraulic head.

Even if the model is not very sensitive to some parameters, their cumulative effect may be significant. Evapotranspiration in the model was assigned a uniform value (constant extinct depth and constant maximum evapotranspiration rate) over the whole LRB. Factors affecting groundwater evaporation, such as land use type and vadose zone porosity, were not fully taken into account in the model. Specific storage and specific yield were important parameters in the transient model, but they were set as constants for each type of the aquifer material. Similar to hydraulic conductivity, specific storage also decreases with depth (Kuang et al., 2021). The decrease of specific storage with depth was not taken into account in the transient model.

The water table observation data used in the model calibration also have some uncertainties. As the water table observation data were obtained from pumping wells, the water table were affected by the groundwater withdrawal. The observed water tables are lower than the natural values without groundwater withdrawal. In addition, the measured water table data are all located in the Lhasa city, because there is no well in the remaining portions of the study area. The lack of water table observation data will also lead to some uncertainties of the model.

4.2. Limitations

This study made the first attempt to construct a numerical groundwater flow model coupled with the effects of glacier and permafrost for the LRB. Due to the scarce groundwater literature in this alpine region and the not abundant observation data to calibrate the model, there are some limitations in the current model. First, the transient model coupling future climate change was built based on the steady-state model and the calibration of the transient model (*Fit-NRMSE* = 0.74) is not good as the steady-state model (*Fit-NRMSE* = 0.96). The calibration targets come from annual baseflow separation and no baseflow time series are available for model calibration. The model also cannot reflect the glacier and permafrost changes due to climate warming. An accurate groundwater recharge rate from glaciers is yet to be clarified as the climate warming. The influence of seasonal permafrost freeze-thaw processes and the thaw of permafrost due to future climate warming are not considered. In addition to the influence of precipitation, there are many other factors such as evaporation, temperature, and radiation that will affect the groundwater flow system in the future climate change scenarios. Ignoring these factors will reduce the reliability of the prediction results of the model.

Despite these limitations and uncertainties of the current model, the results agree with observation data and provide preliminarily the interactions between groundwater and surface water. The model also provides for the first time the patterns of the groundwater flow system and the response of the groundwater system to future climate change in the LRB.

5. Conclusions

A three-dimensional numerical groundwater flow model was built for the LRB accounting for precipitation, evapotranspiration, land use, glacier, and permafrost. The model was calibrated by baseflow data during winter-dry season and water table observed in pumping wells in the Lhasa city. Reasonable agreement is achieved (*Fit-NRMSE* = 0.96) between simulated and measured data. Response of the groundwater flow system to future climate change was also predicted based on different future climate changes scenarios.

Results show that about 13.6 % of precipitation infiltrates and becomes groundwater. More than 80 % of the groundwater flow within depth less than 0.3 km below the ground surface. Baseflow is the most important component of the model. About 93.4 % of the groundwater discharges to streams as baseflow, 5.5 % evaporates and 1.1 % flow out through the southern boundary. The overall recharge of glacier meltwater to groundwater is 10 % of the total groundwater recharge across the LRB. Most groundwater flow within localized flow systems with tracking time less than 100 years and tracking distance shorter than 10 km.

The predicted baseflow and mean hydraulic head fluctuate with the variation of future annual precipitation in 2020–2100. Both baseflow and mean hydraulic head increase with precipitation in the different future climate change scenarios. The increasing trends in baseflow for the four scenarios range from 0.07 to 0.21 m^3/s per year during 2020–2100. The baseflow variation will become greater in the future as wet year will become wetter and dry year will become drier.

Groundwater flow pattern and interactions between groundwater and surface water are important to an improved water resources management and sustainable water usage in the LRB. Studies on groundwater in the LRB are becoming even more important due to climate warming. Groundwater flow model construction for such alpine areas with limited observation data and previous studies is still an unresolved issue. This study makes the first attempt to build a groundwater flow model. Results of this study will help construct numerical groundwater flow models in river basins with geological and hydrogeological characteristics similar to the LRB on the Tibetan Plateau and other alpine regions.

CRediT authorship contribution statement

Jiachang Chen: Model, Writing-original draft. **Xingxing Kuang:** Conceptualization, Writing - review & editing, Funding acquisition. **Michele Lancia:** Data analysis, Writing - review & editing. **Yingying Yao:** Data analysis, Writing - review & editing. **Chunmiao Zheng:** Writing - review & editing, Funding acquisition.

Declaration of Competing Interest

The authors report no declarations of interest.

Acknowledgements

This research was supported by the National Natural Science Foundation of China (Grant No. 91747204), Guangdong Provincial Key Laboratory of Soil and Groundwater Pollution Control (No. 2017B030301012), the Strategic Priority Research Program of Chinese Academy of Sciences (Grant XDA20060402), High-level Special Funding of the Southern University of Science and Technology (Grant No. G02296302, G02296402) and an AXA Research Fund Post-Doctoral Fellowship awarded to X.K.

Appendix A. Supplementary data

Supplementary material related to this article can be found, in the online version, at doi:https://doi.org/10.1016/j.ejrh.2021.100871.

References

Andermann, C., Longuevergne, L., Bonnet, S., Crave, A., Davy, P., Gloaguen, R., 2012. Impact of transient groundwater storage on the discharge of Himalayan rivers. Nat. Geosci. 5 (2), 127–132. https://doi.org/10.1038/ngeo1356.

Banta, E.R., 2000. MODFLOW-2000, The U.S. Geological Survey Modular Ground-water Model; Documentation of Packages for Simulating Evapotranspiration with a Segmented Function (ETS1) and Drains With Return Flow (DRT1). http://water.usgs.gov/nrp/gwsoftware/modflow2000/ofr00-466.pdf.

Bense, V.F., Person, M.A., 2008. Transient hydrodynamics within intercratonic sedimentary basins during glacial cycles. J. Geophys. Res.-Solid Earth 113, F04005. https://doi.org/10.1029/2007JF000969.

Bianduo, Bianbaciren, Li, L., Wang, W., Zhaxiyangzong, 2009. The response of lake change to climate fluctuation in north Qinghai-Tibet Plateau in last 30 years. J. Geogr. Sci. 19 (2), 131–142. https://doi.org/10.1007/s11442-009-0131-z.

Bibi, S., Wang, L., Li, X., Zhou, J., Chen, D., Yao, T., 2018. Climatic and associated cryospheric, biospheric, and hydrological changes on the Tibetan Plateau: a review. Int. J. Climatol. 38 (S1), e1–e17. https://doi.org/10.1002/joc.5411.

Bookhagen, B., Burbank, D.W., 2010. Toward a complete Himalayan hydrological budget: spatiotemporal distribution of snowmelt and rainfall and their impact on river discharge. J. Geophys. Res.-Earth Surf. 115 (F3), F03019. https://doi.org/10.1029/2009JF001426.

Boulton, G.S., Caban, P.E., Van Gijssel, K., 1995. Groundwater flow beneath ice sheets: part I - large scale patterns. Quat. Sci. Rev. 14 (6), 545–562. https://doi.org/10.1016/0277-3791(95)00039-R.

Breemer, C.W., Clark, P.U., Haggerty, R., 2002. Modeling the subglacial hydrology of the late Pleistocene Lake Michigan Lobe, Laurentide Ice Sheet. Geol. Soc. Am. Bull. 114 (6), 665–674. https://doi.org/10.1130/0016-7606(2002)114<0665:MTSHOT>2.0.CO;2.

Cao, G., Zheng, C., Scanlon, B., Liu, J., Li, W., 2013. Use of flow modeling to assess sustainability of groundwater resources in the North China Plain. Water Resour. Res. 49 (1), 159–175. https://doi.org/10.1029/2012WR011899.

Carlson, A.E., Jenson, J.W., Clark, P.U., 2007. Modeling the subglacial hydrology of the James Lobe of the Laurentide Ice Sheet. Quat. Sci. Rev. 26 (9), 1384–1397. https://doi.org/10.1016/j.quascirev.2007.02.002.

Chen, J., Mei, Y., Xiao, W., 2019. Establishment of the ecological relationships and properties of the Lhasa River Basin water resources system, China. Sustain. Cities Soc. 47, 101477. https://doi.org/10.1016/j.scs.2019.101477.

Cheng, G., Jin, H., 2013. Permafrost and groundwater on the Qinghai-Tibet Plateau and in northeast China. Hydrogeol. J. 21 (1), 5–23. https://doi.org/10.1007/s10040-012-0927-2.

Cheng, G., Wu, T., 2007. Responses of permafrost to climate change and their environmental significance, Qinghai-Tibet Plateau. J. Geophys. Res.-Earth Surf. 112 (F2) https://doi.org/10.1029/2006JF000631.

Cohen, D., Person, M., Wang, P., Gable, C.W., Hutchinson, D., Marksamer, A., Dugan, B., Kooi, H., Groen, K., Lizarralde, D., Evans, R.L., Day-Lewis, F.D., Lane, J.W., 2010. Origin and extent of fresh paleowaters on the Atlantic continental shelf, USA. Ground Water 48 (1), 143–158. https://doi.org/10.1111/j.1745-6584.2009.00627.x.

de Graaf, I.E.M., Gleeson, T., van Beek, L.P.H., Sutanudjaja, E.H., Bierkens, M.F.P., 2019. Environmental flow limits to global groundwater pumping. Nature 574 (7776), 90–94. https://doi.org/10.1038/s41586-019-1594-4.

Duan, A.M., Wu, G.X., 2006. Change of cloud amount and the climate warming on the Tibetan Plateau. Geophys. Res. Lett. 33 (22), L22704. https://doi.org/10.1029/2006GL027946.

Duan, Q., Sorooshian, S., Gupta, V.K., 1994. Optimal use of the SCE-UA global optimization method for calibrating watershed models. J. Hydrol. 158 (3), 265–284. https://doi.org/10.1016/0022-1694(94)90057-4.

Evans, S.G., Ge, S., Liang, S., 2015. Analysis of groundwater flow in mountainous, headwater catchments with permafrost. Water Resour. Res. 51 (12), 9564–9576. https://doi.org/10.1002/2015WR017732.

Feng, Y., 2015. Quantitative Analysis and Eco-Hydrology Effects of the Variation of Permafrost in the Qinghai-Tibetan Plateau (in Chinese with English Abstract). Master Thesis. China University of Geosciences (Beijing), Beijing, China.

Fetter, C.W., 2001. Applied Hydrogeology. Prentice Hall, Upper Saddle River.

Gao, Y., Cuo, L., Zhang, Y., 2014. Changes in moisture flux over the Tibetan Plateau during 1979-2011 and possible mechanisms. J. Clim. 27 (5), 1876–1893. https://doi.org/10.1175/JCLI-D-13-00321.1.

Gao, H., Wang, J., Yang, Y., Pan, X., Ding, Y., Duan, Z., 2021a. Permafrost hydrology of the Qinghai-Tibet Plateau: a review of processes and modeling. Front. Earth Sci. 8, 576838. https://doi.org/10.3389/feart.2020.576838.

Gao, Z., Niu, F., Wang, Y., Lin, Z., Wang, W., 2021b. Suprapermafrost groundwater flow and exchange around a thermokarst lake on the Qinghai–Tibet Plateau, China. J. Hydrol. 593, 125882. https://doi.org/10.1016/j.jhydrol.2020.125882.

Ge, S., Wu, Q., Lu, N., Jiang, G., Ball, L., 2008. Groundwater in the Tibet Plateau, western China. Geophys. Res. Lett. 35 (18), L18403. https://doi.org/10.1029/2008GL034809.

Ge, S.M., McKenzie, J., Voss, C., Wu, Q.B., 2011. Exchange of groundwater and surface-water mediated by permafrost response to seasonal and long term air temperature variation. Geophys. Res. Lett. 38, L14402. https://doi.org/10.1029/2011GL047911.

Gleeson, T., Smith, L., Moosdorf, N., Hartmann, J., Durr, H.H., Manning, A.H., van Beek, L.P.H., Jellinek, A.M., 2011. Mapping permeability over the surface of the Earth. Geophys. Res. Lett. 38, L02401. https://doi.org/10.1029/2010GL045565.

Goderniaux, P., Brouyere, S., Blenkinsop, S., Burton, A., Fowler, H.J., Orban, P., Dassargues, A., 2011. Modeling climate change impacts on groundwater resources using transient stochastic climatic scenarios. Water Resour. Res. 47, W12516. https://doi.org/10.1029/2010WR010082.

Green, T.R., Taniguchi, M., Kooi, H., Gurdak, J.J., Allen, D.M., Hiscock, K.M., Treidel, H., Aureli, A., 2011. Beneath the surface of global change: impacts of climate change on groundwater. J. Hydrol. 405 (3–4), 532–560. https://doi.org/10.1016/j.jhydrol.2011.05.002.

Haitjema, H.M., Mitchell-Bruker, S., 2005. Are water tables a subdued replica of the topography? Ground Water 43 (6), 781–786. https://doi.org/10.1111/j.1745-6584.2005.00090.x.

Harbaugh, A.W., 2005. MODFLOW-2005, The U.S. Geological Survey Modular Ground-Water Model - The Ground-Water Flow Process: U.S. Geological Survey Techniques and Methods 6-A16.

Hu, L.T., Jiao, J.J., 2015. Calibration of a large-scale groundwater glow model using GRACE data: a case study in the Qaidam Basin, China. Hydrogeol. J. 23, 1305–1317. https://doi.org/10.1007/s10040-015-1278-6.

Huang, Q., Long, D., Du, M., Han, Z., Han, P., 2020. Daily continuous river discharge estimation for ungauged basins using a hydrologic model calibrated by satellite altimetry: implications for the SWOT mission. Water Resour. Res. 56 https://doi.org/10.1029/2020WR027309 e2020WR027309.

Huss, M., Hock, R., 2018. Global-scale hydrological response to future glacier mass loss. Nat. Clim. Change 8, 135–140. https://doi.org/10.1038/s41558-017-0049-x.

Immerzeel, W.W., van Beek, L.P., Bierkens, M.F., 2010. Climate change will affect the Asian water towers. Science 328 (5984), 1382–1385. https://doi.org/10.1126/science.1183188.

Jasechko, S., Perrone, D., 2021. Global groundwater wells at risk of running dry. Science 372 (6540), 418–421. https://doi.org/10.1126/science.abc2755.

Kang, S., Xu, Y., You, Q., Flügel, W.-A., Pepin, N., Yao, T., 2010. Review of climate and cryospheric change in the Tibetan Plateau. Environ. Res. Lett. 5 (1), 015101. https://doi.org/10.1088/1748-9326/5/1/015101.

Kirshen, P.H., 2002. Potential impacts of global warming on groundwater in eastern Massachusetts. J. Water Res. Plann. Manage. 128 (3), 216–226. https://doi.org/10.1061/(ASCE)0733-9496(2002)128:3(216).

Kuang, X., Jiao, J.J., 2014. An integrated permeability-depth model for Earth's crust: permeability of Earth's crust. Geophys. Res. Lett. 41 (21), 7539–7545. https://doi.org/10.1002/2014GL061999.

Kuang, X., Jiao, J.J., 2016. Review on climate change on the Tibetan Plateau during the last half century. J. Geophys. Res.-Atmos. 121 (8), 3979–4007. https://doi.org/10.1002/2015JD024728.

Kuang, X., Zheng, C., Jiao, J.J., Cherry, J.A., Chen, J., 2021. An empirical specific storage-depth model for the Earth's crust. J. Hydrol. 592, 125784. https://doi.org/10.1016/j.jhydrol.2020.125784.

Kurylyk, B.L., MacQuarrie, K.T.B., McKenzie, J.M., 2014. Climate change impacts on groundwater and soil temperatures in cold and temperate regions: implications, mathematical theory, and emerging simulation tools. Earth-Sci. Rev. 138313–138334.

Kurylyk, B.L., Hayashi, M., Quinton, W.L., McKenzie, J.M., Voss, C.I., 2016. Influence of vertical and lateral heat transfer on permafrost thaw, peatland landscape transition, and groundwater flow. Water Resour. Res. 52 (2), 1286–1305. https://doi.org/10.1002/2015WR018057.

Langridge, R., Daniels, B., 2017. Accounting for climate change and drought in implementing sustainable groundwater management. Water Resour. Manage. 31 (11), 3287–3298. https://doi.org/10.1007/s11269-017-1607-8.

Lemieux, J.M., Sudicky, E.A., Peltier, W.R., Tarasov, L., 2008. Simulating the impact of glaciations on continental groundwater flow systems: 1. Relevant processes and model formulation. J. Geophys. Res.-Earth 113, F03017. https://doi.org/10.1029/2007JF000928.

Li, X., Cheng, G., Jin, H., Kang, E., Che, T., Jin, R., Wu, L., Nan, Z., Wang, J., Shen, Y., 2008. Cryospheric change in China. Glob. Planet. Change 62 (3–4), 210–218. https://doi.org/10.1016/j.gloplacha.2008.02.001.

Liang, X., Xie, Z., 2001. A new surface runoff parameterization with subgrid-scale soil heterogeneity for land surface models. Adv. Water Resour. 24 (9–10), 1173–1193. https://doi.org/10.1016/S0309-1708(01)00032-X.

Liang, X., Wood, E.F., Lettenmaier, D.P., 1996. Surface soil moisture parameterization of the VIC-2L model: evaluation and modification. Glob. Planet. Change 13 (1–4), 195–206. https://doi.org/10.1016/0921-8181(95)00046-1.

Lin, X., Zhang, Y., Yao, Z., Gong, T., Wang, H., Chu, D., Liu, L., Zhang, F., 2008. The trend on runoff variations in the Lhasa River Basin. J. Geogr. Sci. 18 (1), 95–106. https://doi.org/10.1007/s11442-008-0095-4.

Liu, T., 1999. Hydrological characteristics of Yalungzangbo river (in Chinese with English abstract). Acta Geogr. Sin. 66 (S1), 157–164. https://doi.org/10.11821/dlxb201409004.

Liu, J., 2019. Remote Sensing Monitoring Dataset of Land Use Status in Six Provinces in Western China for Many Years (1970s, 1980s, 1995, 2000, 2005, 2010, 2015). National Tibetan Plateau Data Center. https://doi.org/10.11888/Socioeco.tpdc.270469.

Liu, X., Chen, B., 2000. Climatic warming in the Tibetan Plateau during recent decades. Int. J. Climatol. 20 (14), 1729–1742. https://doi.org/10.1002/1097-0088(20001130)20:14<1729::AID-JOC556>3.0.CO;2-Y.

Liu, J., Xie, J., Gong, T., Wang, H., Xie, Y., 2011. Impacts of winter warming and permafrost degradation on water variability, upper Lhasa River, Tibet. Quat. Int. 244 (2), 178–184. https://doi.org/10.1016/j.quaint.2010.12.018.

Liu, W., Xu, Z., Li, F., Zhang, L., Zhao, J., Yang, H., 2015. Impacts of climate change on hydrological processes in the Tibetan Plateau: a case study in the Lhasa River basin. Stoch. Environ. Res. Risk Assess. 29 (7), 1809–1822. https://doi.org/10.1007/s00477-015-1066-9.

Liu, J., Gao, Z., Wang, M., Li, Y., Yu, C., Shi, M., Zhang, H., Ma, Y., 2019. Stable isotope characteristics of different water bodies in the Lhasa River Basin. Environ. Earth Sci. 78, 71. https://doi.org/10.1007/s12665-019-8078-6.

Ma, R., Sun, Z., Hu, Y., Chang, Q., Wang, S., Xing, W., Ge, M., 2017. Hydrological connectivity from glaciers to rivers in the Qinghai-Tibet Plateau: roles of suprapermafrost and subpermafrost groundwater. Hydrol. Earth Syst. Sci. Discuss. 21 (9), 4803–4823. https://doi.org/10.5194/hess-21-4803-2017.

Mackay, J.D., Barrand, N.E., Hannah, D.M., Krause, S., Jackson, C.R., Everest, J., MacDonald, A.M., Dochartaigh, B.ÉÓ, 2020. Proglacial groundwater storage dynamics under climate change and glacier retreat. Hydrol. Process. 34 (26), 5456–5473. https://doi.org/10.1002/hyp.13961.

Markovich, K.H., Maxwell, R.M., Fogg, G.E., 2016. Hydrogeological response to climate change in alpine hillslopes. Hydrol. Process. 30 (18), 3126–3138. https://doi.org/10.1002/hyp.10851.

Niswonger, R.G., Panday, S., Ibaraki, M., 2011. MODFLOW-NWT, A Newton Formulation for MODFLOW-2005. U.S. Geological Survey Techniques and Methods 6-A37, 44 p.

Normani, S.D., Sykes, J.F., 2012. Paleohydrogeologic simulations of Laurentide ice-sheet history on groundwater at the eastern flank of the Michigan Basin. Geofluids 12 (1), 97–122. https://doi.org/10.1111/j.1468-8123.2012.00362.x.

O'Neill, B.C., Tebaldi, C., van Vuuren, D.P., Eyring, V., Friedlingstein, P., Hurtt, G., Knutti, R., Kriegler, E., Lamarque, J.-F., Lowe, J., Meehl, G.A., Moss, R., Riahi, K., Sanderson, B.M., 2016. The scenario model intercomparison project (ScenarioMIP) for CMIP6. Geosci. Model. Dev. Discuss. 9, 3461–3482. https://doi.org/10.5194/gmd-9-3461-2016.

Okello, A.M.L.S., Uhlenbrook, S., Jewitt, G.P.W., Masih, I., Riddell, E.S., Van der Zaag, P., 2018. Hydrograph separation using tracers and digital filters to quantify runoff components in a semi-arid mesoscale catchment. Hydrol. Process. 32 (10), 1334–1350. https://doi.org/10.1002/hyp.11491.

Peng, D., Du, Y., 2010. Comparative analysis of several Lhasa River Basin flood forecast models in Yarlung Zangbo River. 2010 4th International Conference on Bioinformatics and Biomedical Engineering 1–4.

Prasch, M., 2010. Distributed Process Oriented Modelling of the Future Impact of Glacier Melt Water on Runoff in the Lhasa River Basin in Tibet. PhD Thesis. Ludwig-Maximillians-University of Munich, Germany.

Price, K., 2011. Effects of watershed topography, soils, land use, and climate on baseflow hydrology in humid regions: a review. Prog. Phys. Geogr. 35 (4), 465–492. https://doi.org/10.1177/0309133311402714.

Provost, A.M., Voss, C.I., Neuzil, C.E., 2012. Glaciation and regional groundwater flow in the Fennoscandian shield. Geofluids 12 (1), 79–96. https://doi.org/10.1111/j.1468-8123.2012.00361.x.

QGIS Development Team, 2020. QGIS Geographic Information System. Open Source Geospatial Foundation Project. http://qgis.osgeo.org.

Qiu, L., You, J., Qiao, F., Peng, D., 2014. Simulation of snowmelt runoff in ungauged basins based on MODIS: a case study in the Lhasa River basin. Stoch. Environ. Res. Risk Assess. 28 (6), 1577–1585. https://doi.org/10.1007/s00477-013-0837-4.

Ran, Y., Li, X., Cheng, G., Nan, Z., Che, J., Sheng, Y., Wu, Q., Jin, H., Luo, D., Tang, Z., Wu, X., 2021. Mapping the permafrost stability on the Tibetan Plateau for 2005–2015. Sci. China Earth Sci. 64, 62–79. https://doi.org/10.1007/s11430-020-9685-3.

Saberi, L., McLaughlin, R.T., Zhi, W., Li, L., Mark, B.G., 2019. Multi-scale temporal variability in meltwater contributions in a tropical glacierized watershed. Hydrol. Earth Syst. Sci. Discuss. 23, 405–425. https://doi.org/10.5194/hess-23-405-2019.

Scanlon, B.R., Keese, K.E., Flint, A.L., Flint, L.E., Gaye, C.B., Edmunds, W.M., Simmers, I., 2006. Global synthesis of groundwater recharge in semiarid and arid regions. Hydrol. Process. 20 (15), 3335–3370. https://doi.org/10.1002/hyp.6335.

Shi, H., Fu, X., Chen, J., Wang, G., Li, T., 2014. Spatial distribution of monthly potential evaporation over mountainous regions: case of the Lhasa River basin, China. Hydrol. Sci. J. 59 (10), 1856–1871. https://doi.org/10.1080/02626667.2014.881486.

Shi, R., Yang, H., Yang, D., 2020. Spatiotemporal variations in frozen ground and their impacts on hydrological components in the source region of the Yangtze River. J. Hydrol. 590, 125237. https://doi.org/10.1016/j.jhydrol.2020.125237.

Singh, P., Jain, S.K., 2003. Modelling of streamflow and its components for a large Himalayan basin with predominant snowmelt yields. Hydrol. Sci. J. Des Sci. Hydrol. 48 (2), 257–276. https://doi.org/10.1623/hysj.48.2.257.44693.

Somers, L.D., McKenzie, J.M., Mark, B.G., Lagos, P., G-HC, Ng, Wickert, A.D., Yarleque, C., Baraër, M., Silva, Y., 2019. Groundwater buffers decreasing glacier melt in an andean watershed—but not forever. Geophys. Res. Lett. 46 (22), 13016–13026. https://doi.org/10.1029/2019GL084730.

Tague, C., Grant, G.E., 2009. Groundwater dynamics mediate low-flow response to global warming in snow-dominated alpine regions. Water Resour. Res. 45, W07421. https://doi.org/10.1029/2008WR007179.

Tibet Geological Survey, 1979. Synthetic Hydrogeological Map Republic of China. H-46 Series Scale 1:1,000,000. China Geological Survey.

Tongal, H., Demirel, M.C., Booij, M.J., 2013. Seasonality of low flows and dominant processes in the Rhine River. Stoch. Environ. Res. Risk Assess. 27 (2), 498–503. https://doi.org/10.1007/s00477-012-0594-9.

van Weert, F.H.A., van Gijssel, K., Leijnse, A., Boulton, G.S., 1997. The effects of Pleistocene glaciations on the geohydrological system of Northwest Europe. J. Hydrol. 195 (1–4), 137–159. https://doi.org/10.1016/S0022-1694(96)03248-9.

Walvoord, M.A., Voss, C.I., Wellman, T.P., 2012. Influence of permafrost distribution on groundwater flow in the context of climate-driven permafrost thaw: example from Yukon Flats Basin, Alaska, United States. Water Resour. Res. 48, W07524. https://doi.org/10.1029/2011WR011595.

Wang, J., Wang, F., 2020. Discussion on the range of groundwater depression cone, radius of influence and scope of environmental impacts during pumping. J. Hydraul. Eng.-ASCE 51 (7), 827–834. https://doi.org/10.13243/j.cnki.slxb.20200112.

Wang, X., Chen, R., Liu, G., Han, C., Yang, Y., Song, Y., Liu, J., Liu, Z., Liu, X., Guo, S., Wang, L., Zheng, Q., 2019. Response of low flows under climate warming in high-altitude permafrost regions in western China. Hydrol. Process. 33 (1), 66–75. https://doi.org/10.1002/hyp.13311.

Wu, S., Yin, Y., Zheng, D., Yang, Q., 2005. Aridity/humidity status of land surface in China during the last three decades. Sci. China Ser. D-Earth Sci. 48 (9), 1510–1518. https://doi.org/10.1360/04yd0009.

Wu, Z., Mei, Y., Chen, J., Hu, T., Xiao, W., 2019. Attribution analysis of dry season runoff in the Lhasa River using an extended hydrological sensitivity method and a hydrological model. Water 11 (6), 1187.

Xiang, L., Wang, H., Steffen, H., Wu, P., Jia, L., Jiang, L., Shen, Q., 2016. Groundwater storage changes in the Tibetan Plateau and adjacent areas revealed from GRACE satellite gravity data. Earth Planet. Sci. Lett. 452, 309. https://doi.org/10.1016/j.epsl.2016.08.021.

Xiao, C., Liu, S., Zhao, L., Wu, Q., Li, P., Liu, C., Zhang, Q., Ding, Y., Yao, T., Li, Z., Pu, J., 2007. Observed changes of cryosphere in China over the second half of the 20th century: an overview. Ann Glaciol. 46, 382–390. https://doi.org/10.3189/172756407782871396.

Yang, W., Xiao, C., Liang, X., Zhang, Z., 2019. Two baseflow separation methods based on daily average gage height and discharge. Water Sci. Tech.-Water Supply 19 (7), 1978–1985. https://doi.org/10.2166/ws.2019.074.

Yao, T., Wang, Y., Liu, S., Pu, J., Shen, Y., Lu, A., 2004. Recent glacial retreat in High Asia in China and its impact on water resource in Northwest China. Sci. China Ser. D Earth Sci. 47 (12), 1065–1075. https://doi.org/10.1360/03yd0256.

Yao, T., Pu, J., Lu, A., Wang, Y., Yu, W., 2007. Recent glacial retreat and its impact on hydrological processes on the tibetan plateau, China, and sorrounding regions. Arct. Antarct. Alp. Res. 39 (4), 642–650. https://doi.org/10.1657/1523-0430(07-510)[YAO]2.0.CO;2.

Yao, T., Thompson, L., Yang, W., Yu, W., Gao, Y., Guo, X., Yang, X., Duan, K., Zhao, H., Xu, B., Pu, J., Lu, A., Xiang, Y., Kattel, D., Joswiak, D., 2012. Different glacier status with atmospheric circulations in Tibetan Plateau and surroundings. Nat. Clim. Change 2 (9), 663–667. https://doi.org/10.1038/nclimate1580.

Yao, Y., Zheng, C., Andrews, C., Zheng, Y., Zhang, A., Liu, J., 2017. What controls the partitioning between baseflow and mountain block recharge in the Qinghai-Tibet Plateau? Geophys. Res. Lett. 44 (16), 8352–8358. https://doi.org/10.1002/2017GL074344.

Yao, Y., Zheng, C., Andrews, C.B., Scanlon, B.R., Kuang, X., Zeng, Z., Jeong, S.-J., Lancia, M., Wu, Y., Li, G., 2021. Role of groundwater in sustaining northern Himalayan rivers. Geophys. Res. Lett. 48 https://doi.org/10.1029/2020GL092354 e2020GL092354.

Zhang, D., Huang, J., Guan, X., Chen, B., Zhang, L., 2013. Long-term trends of precipitable water and precipitation over the Tibetan Plateau derived from satellite and surface measurements. J. Quant. Spectrosc. Radiat. Transfer 122, 64–71. https://doi.org/10.1016/j.jqsrt.2012.11.028.

Zhang, L., Brutsaert, W., Crosbie, R., Potter, N., 2014. Long-term annual groundwater storage trends in Australian catchments. Adv. Water Resour. 74, 156–165. https://doi.org/10.1016/j.advwatres.2014.09.001.

Zou, D., Zhao, L., Sheng, Y., Chen, J., Hu, G., Wu, T., Wu, J., Xie, C., Wu, X., Pang, Q., Wang, W., Du, E., Li, W., Liu, G., Li, J., Qin, Y., Qiao, Y., Wang, Z., Shi, J., Cheng, G., 2017. A new map of permafrost distribution on the Tibetan Plateau. Cryosphere 11 (6), 2527–2542. https://doi.org/10.5194/tc-11-2527-2017.